

Loss of 26S Proteasome Function Leads to Increased Cell Size and Decreased Cell Number in Arabidopsis Shoot Organs¹[C][W][OA]

Jasmina Kurepa, Songhu Wang, Yan Li, David Zaitlin, Andrew J. Pierce, and Jan A. Smalle*

Plant Physiology, Biochemistry, and Molecular Biology Program, Department of Plant and Soil Sciences, College of Agriculture, University of Kentucky, Lexington, Kentucky 40546 (J.K., S.W., Y.L., J.A.S.); Kentucky Tobacco Research and Development Center, University of Kentucky, Lexington, Kentucky 40546 (D.Z.); and Department of Microbiology, Immunology, and Molecular Genetics, College of Medicine, University of Kentucky, Lexington, Kentucky 40546 (A.J.P.)

Although the final size of plant organs is influenced by environmental cues, it is generally accepted that the primary size determinants are intrinsic factors that regulate and coordinate cell proliferation and cell expansion. Here, we show that optimal proteasome function is required to maintain final shoot organ size in Arabidopsis (*Arabidopsis thaliana*). Loss of function of the subunit regulatory particle AAA ATPase (RPT2a) causes a weak defect in 26S proteasome activity and leads to an enlargement of leaves, stems, flowers, fruits, seeds, and embryos. These size increases are a result of increased cell expansion that compensates for a reduction in cell number. Increased ploidy levels were found in some but not all enlarged organs, indicating that the cell size increases are not caused by a higher nuclear DNA content. Partial loss of function of the regulatory particle non-ATPase (RPN) subunits RPN10 and RPN12a causes a stronger defect in proteasome function and also results in cell enlargement and decreased cell proliferation. However, the increased cell volumes in *rpn10-1* and *rpn12a-1* mutants translated into the enlargement of only some, but not all, shoot organs. Collectively, these data show that during Arabidopsis shoot development, the maintenance of optimal proteasome activity levels is important for balancing cell expansion with cell proliferation rates.

The 26S proteasome (26SP) is a multisubunit, multicatalytic, 2.4-MD protease responsible for the degradation of proteins involved in various biological processes (Varshavsky, 2005; DeMartino and Gillette, 2007; Hanna and Finley, 2007; Kurepa and Smalle, 2008). Prior to their degradation, most 26SP target proteins are covalently modified with a polyubiquitin chain in a three-step enzymatic reaction (Smalle and Vierstra, 2004). In addition to its central function in recognizing and degrading polyubiquitinated proteins, the 26SP can also degrade proteins that were not modified by polyubiquitination (Benaroudj et al.,

2001; Asher et al., 2006; Asher and Shaul, 2006; Lee et al., 2006; Pande et al., 2007).

The 26SP consists of a cylindrical 20S core complex and two 19S regulatory particles that cap the 20S core on both ends. The 20S proteasome (20SP) is composed of seven related α -subunits and seven related β -subunits arranged in a stack of four heptameric rings. The outer rings are composed of α -subunits and the inner rings are composed of β -subunits, of which three have proteolytic activities described as caspase-, trypsin-, and chymotrypsin-like (Kurepa and Smalle, 2008). The regulatory particles (RPs) serve as highly restrictive gatekeepers for the core protease. Each RP is composed of a lid subcomplex, which contains at least nine non-ATPase subunits designated RPN3, RPN5 to RPN9, RPN11, RPN12, and RPN15 and a base subcomplex that contains RPN1, RPN2, RPN13, and RPT1 to RPT6 subunits. The RPN10 and RPN13 subunits have been shown to recognize polyubiquitinated proteins; thus, they define the main interaction points of the 26SP with its target proteins (Young et al., 1998; Smalle and Vierstra, 2004; Husnjak et al., 2008; Kurepa and Smalle, 2008; Schreiner et al., 2008). Ubiquitinated proteins can also interact with the 26SP by first binding to the carrier proteins RAD23 (for radiation sensitive 23), DSK2 (for dominant suppressor of *kar1* 2), and DD11 (for DNA damage inducible 1), which then bind the RP base subunit RPN1 (Elsasser et al., 2002, 2004;

¹ This work was supported by the Kentucky Tobacco Research and Development Center, the U.S. Department of Agriculture Cooperative State Research, Education, and Extension Service (grant no. 2005-35304-16043), and the Kentucky Science and Engineering Foundation (grant no. 148-502-06-189).

* Corresponding author; e-mail jsmalle@uky.edu.

The author responsible for distribution of materials integral to the findings presented in this article in accordance with the policy described in the Instructions for Authors (www.plantphysiol.org) is: Jan A. Smalle (jsmalle@uky.edu).

[C] Some figures in this article are displayed in color online but in black and white in the print edition.

[W] The online version of this article contains Web-only data.

[OA] Open Access articles can be viewed online without a subscription.

www.plantphysiol.org/cgi/doi/10.1104/pp.109.135970

Elsasser and Finley, 2005). The RPT base subunits belong to the class of AAA ATPases and are thought to be important for the unfolding and translocation of substrate proteins through the central pore in the 20SP base called the 20SP gate (Vale, 2000; Bajorek and Glickman, 2004). Similar to all other AAA ATPases, the non-AAA modules of RPTs confer functional specificity to these proteins, and in yeast, the functions of the six RP ATPases have been shown to differ (Smith et al., 2007). For example, the main function of yeast RPT2 and RPT5 subunits is to regulate the opening of the 20SP gate (Smith et al., 2007).

Despite the many recent advances in proteasome research (Husnjak et al., 2008; Kurepa and Smalle, 2008; Schreiner et al., 2008), the specific functions of most of the RP subunits remain unknown. Because of the complex quaternary structure of the 26SP and the feedback mechanisms that coregulate the expression of proteasome subunit genes in response to temporal or spatial demands, the overexpression of individual subunits in most cases does not lead to a change in total proteasome activity (Kurepa and Smalle, 2008). Thus, the main strategy used to study the specific functions of a particular RP subunit involves the analyses of mutants in which the expression of the corresponding subunit gene is down-regulated or abolished (Kurepa and Smalle, 2008). However, assigning a specific function to an RP subunit based on the analyses of loss-of-function mutants can be difficult. The major challenge in this approach has been to discern between the effects of a mutation on subunit function in particular and on total proteasome function in general. For example, the *halted root (hlt)* mutant was isolated as a short-root mutant that has an expanded root tip, and this phenotype was shown to be a result of a 13-bp-long deletion in the *RPT2a* gene (Ueda et al., 2004). However, the majority of RP mutants described to date have shorter roots, which suggests that it is the down-regulation of 26SP function and not specifically the RPT2a subunit that leads to the change in root growth (Kurepa et al., 2008). In another example, the *ae3-1* mutant, isolated as an enhancer of *asymmetric leaves1 (asl)* and *asl2*, was shown to carry a mutation in the *RPN8a* gene (Huang et al., 2006). The *ae3-1* plants have a reduced rosette size, altered leaf phyllotaxy, and lanceolated, abaxialized leaves (Huang et al., 2006). Double mutant analyses of *asl2* with other proteasome subunit mutants showed that all double mutant lines have comparable leaf phenotypes and, thus, that the originally observed effect of *ae3-1* on *asl1/asl2* phenotypes is the result of a general alteration in 26SP function (Huang et al., 2006). In conclusion, most of the phenotypes of the RP mutants described to date seem to reflect a general alteration in proteasome activity and not a specific defect that relates to a specific function of a particular subunit (Huang et al., 2006; Kurepa et al., 2008).

Comparative analyses of the RP mutants *rpn10-1*, *rpn12a-1*, and *rpt2a-2* revealed that the strongest proteasome defect was caused by *rpn10-1* and the weakest

defect was caused by the *rpt2a-2* mutation (Kurepa et al., 2008). The *rpt2a-2* mutation induces a phenotype that sets this line apart from the other RP mutants: it leads to an increase in size of the rosette and other shoot organs. In this study, we tested the hypothesis that the enlargement of aerial organs in *rpt2a-2* reflects a specific function of the RPT2 subunit. To this end, we determined the cellular phenotypes of two *rpt2a* mutant alleles and compared them with the phenotypes of *rpn10-1* and *rpn12a-1* mutants. We demonstrate that any decrease in 26SP function leads to a reduction in cell number that is accompanied by increased cell sizes. This suggests that optimal proteasome function is required for the proper execution of preprogrammed cell proliferation and expansion rates.

RESULTS

Isolation of Arabidopsis *rpt2* Mutants

In contrast to *Saccharomyces cerevisiae*, *Caenorhabditis elegans*, and *Drosophila melanogaster*, which have one *RPT2* gene, the RPT2 subunit in Arabidopsis (*Arabidopsis thaliana*) is encoded by a two-member gene family (Rubin et al., 1998; Takahashi et al., 2002; Wójcik and DeMartino, 2002; Shibahara et al., 2004; Ueda et al., 2004; Sönnichsen et al., 2005; Kurepa et al., 2008). *AtRPT2a* (At4g29040) and *AtRPT2b* (At2g20140; Fig. 1A) encode 444-amino acid proteins sharing 98.8% identity at the protein level. Analyses of public microarray expression data showed that *RPT2a* is consistently expressed at a higher level than *RPT2b* and that the expression of both genes is developmentally regulated (Fig. 1B).

To analyze the effects of the loss of RPT2 function on shoot growth, we isolated a second ecotype Columbia (Col-0) T-DNA insertion mutation in *RPT2a*, *rpt2a-3*, and an insertion mutation in *RPT2b*. Gel-blot analysis of total RNA revealed that the *RPT2a* transcript level was altered in all tested *rpt2* mutants (Fig. 1C). The weak signal at the migration position of the *RPT2a* transcript in *rpt2a-2* likely represents a cross-reaction of the probe with the *RPT2b* mRNA. In the *rpt2a-3* allele, the transcript was shorter than in the wild type, and sequence analyses of RT-PCR products revealed that it contains the *RPT2a* coding region downstream of the insertion mutation, suggesting that the expression of this transcript is driven by a promoter within the T-DNA (Fig. 1C; data not shown). In the *rpt2b-1* mutant, the *RPT2a* transcript was more abundant than in the wild type, which is in agreement with previously described findings that a potential decrease in proteasome activity leads to a compensatory up-regulation of the expression of 26SP subunit genes (Yang et al., 2004; Huang et al., 2006; Kurepa et al., 2008). We then tested the levels of immunoreactive RPT2 protein in 10-d-old seedlings in all *rpt2* alleles (Fig. 1, D and E). Because RPT2a and RPT2b are nearly identical at the amino acid level, the polyclonal anti-

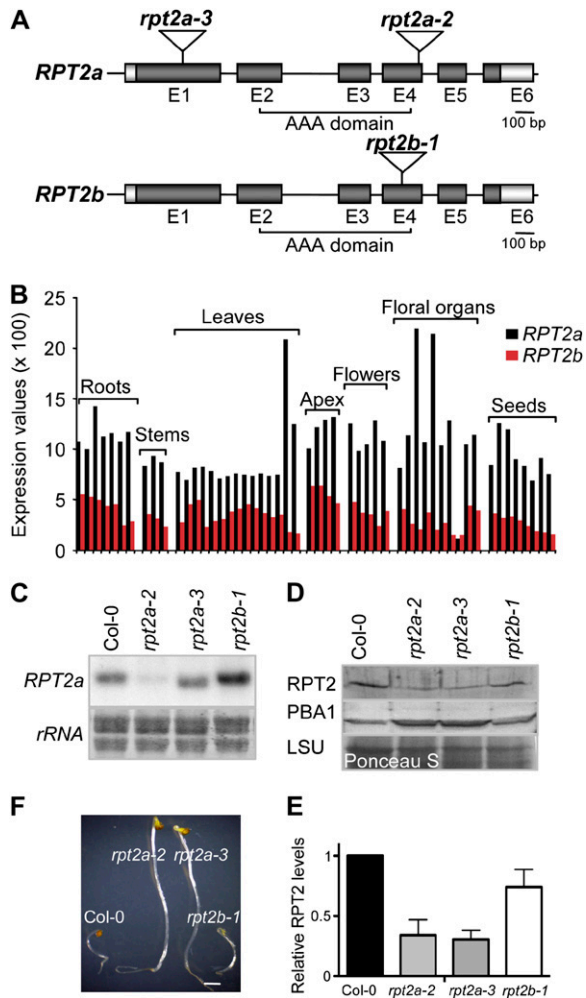


Figure 1. Molecular analyses of *rpt2* mutants. A, *RPT2a* and *RPT2b* gene structures and the positions of the T-DNA insertions. Exons (E) and introns are represented by boxes (dark gray, coding region; light gray, untranslated region) and lines, respectively. Insertion positions of the T-DNA in the *rpt2a-2* (SALK_005596), *rpt2a-3* (SALK_130019), and *rpt2b-1* (SALK_043450C) alleles are shown. B, *RPT2* expression levels during Arabidopsis development. The developmental data set of the AtGen-Express project was used (Schmid et al., 2005). Different bars in the same category denote the different developmental stages as specified by Schmid et al. (2005). C, Expression analyses. RNA gel blots were probed with an *RPT2a* antisense probe. The region of a methylene blue-stained membrane encompassing ribosomal RNAs (*rRNA*) is shown as a loading control. D, *RPT2* protein level in *rpt2a* mutants. Protein extracts from 10-d-old Col-0 and *rpt2* mutant plants were separated by SDS-PAGE, blotted, and probed with anti-*RPT2* and anti-PBA1 antisera. A region of the Ponceau S-stained membrane encompassing the large subunit of Rubisco (LSU) is shown as a loading control. E, Relative levels of *RPT2* protein were assessed by densitometry from four immunoblots. The signal intensity of Col-0 was normalized to 1, and mean values \pm SD are shown. F, MG132 tolerance of *rpt2* mutants. Seeds were sown and grown for 5 d in darkness on water/agar containing 50 μ M MG132. Bar = 1 mm. [See online article for color version of this figure.]

bodies generated against *RPT2a* are expected to recognize both isoforms. In homozygous *rpt2a* mutants, the *RPT2* levels were reduced to 30% \pm 10% of the

wild-type levels, and in *rpt2b-1*, they were reduced to 70% \pm 10%. This suggests that all lines are indeed null mutants and that the *RPT2b* protein represents 30% or less of the total *RPT2* pool in wild-type seedlings. Both *rpt2a* mutants displayed an up-regulation in the abundance of the 20SP subunit PBA1, which is indicative of a loss in 26SP function (Fig. 1D; Yang et al., 2004).

In 26SP RP mutants, decreased 26SP assembly rates lead to an increase in the abundance of the free 20SP, which is further enhanced by the compensatory up-regulation of the proteasome subunit gene set (Kurepa et al., 2008). The increased 20SP activity in *rpt2a-2* and other tested RP mutants leads to an elevated tolerance to the proteasome inhibitor MG132 in a growth response assay (Kurepa et al., 2008). The hypocotyls of 5-d-old etiolated *rpt2a* seedlings were approximately 20% longer than those of wild-type and *rpt2b-1* seedlings (data not shown). Similar to *rpt2a-2* (Kurepa et al., 2008), the *rpt2a-3* mutant was more tolerant to MG132 (Fig. 1F). The hypocotyl elongation of Col-0 seedlings grown on 50 μ M MG132 was inhibited by approximately 80% compared with the untreated control, while the same treatment reduced *rpt2a* hypocotyl growth only approximately 50% compared with the untreated mutants. Two-way nonparametric ANOVA with the Bonferroni posttest confirmed that the effects of the treatment on wild-type and mutant lines were significantly different ($P < 0.0001$). The *rpt2b-1* mutant was not more tolerant to the MG132-induced growth inhibition, however (Fig. 1F). Thus, we concluded that the *rpt2a-2* and *rpt2a-3* mutants share proteasome-related phenotypes both qualitatively and quantitatively.

Morphological Characterization of *rpt2a* Mutants

Due to the low expression level of *RPT2b* compared with *RPT2a* and the relatively weak proteasome defect caused by *rpt2a* mutations, we predicted that the *rpt2b-1* mutant would not show a strong developmental phenotype. Indeed, *rpt2b-1* mutant seedlings were indistinguishable from the wild type (Fig. 2A; data not shown for later developmental stages). In contrast, we noticed that 3-d-old light-grown *rpt2a* mutants had enlarged cotyledons (Fig. 2A). The length and thickness of *rpt2a* roots at this developmental stage were also increased compared with the wild type, but at later stages of development, root growth ceased, similar to the Wassilewskija mutant line *h1r-1/rpt2a-1* (Ueda et al., 2004). Analyses of *rpt2a* embryos revealed that the increased organ size was established already during embryogenesis. In mature embryos, the cotyledon area was 30% \pm 10% larger and the radicle was 30% \pm 10% longer than in the wild type (Fig. 2B; Supplemental Table S1). Since light is an important factor in the control of cell expansion and overall plant morphology, we also measured the dimensions of cotyledons, roots, and hypocotyls of 3-d-old dark-grown *rpt2a* seedlings (Supplemental Table S1). All parts of the etiolated *rpt2a* seedlings were

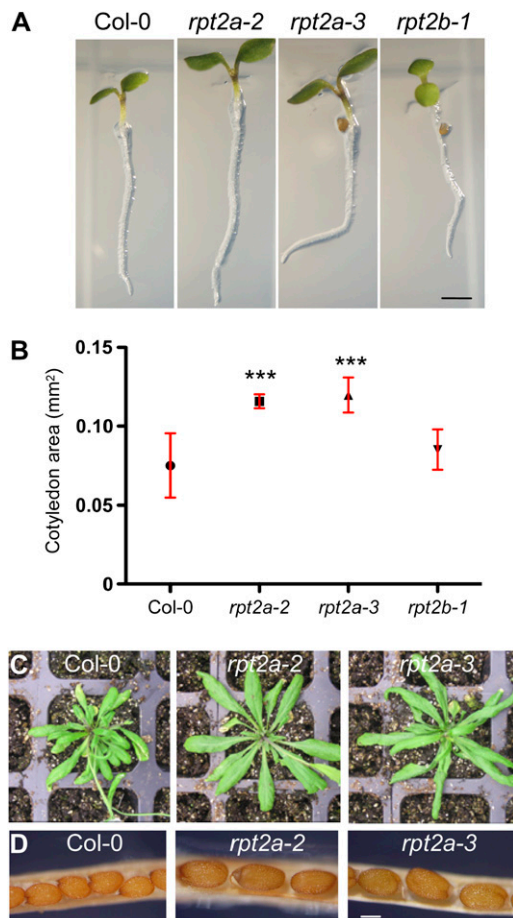


Figure 2. Organ sizes in *rpt2* mutants. A, Phenotypes of 3-d-old *rpt2* mutants grown on vertically positioned MS/2 agar plates. Bar = 1 mm. B, Cotyledon area of mature embryos. Dry seeds were imbibed overnight, cleared with lactophenol, and photographed. A minimum of 20 cotyledons per line was measured. Symbols on the graph represent average values, and the error bars correspond to the sd. *** Significantly different from the wild type ($P \leq 0.0001$). C, Rosette phenotype of *rpt2a* mutants. Seedlings were germinated and grown for 10 d on MS/2 and then transferred to soil. Plants were grown under a long-day photoperiod and photographed 30 d after germination. D, Seed size in *rpt2a* mutants. Mature siliques were dissected, and the central parts of the fruits are shown. Bar = 200 μm .

larger than those in the wild type (approximately 30% increase for root length, approximately 20% for hypocotyl length, approximately 30% for hypocotyl width, and approximately 70% for cotyledon area).

In the *rpt2a* mutants, all shoot organs remained larger than in the wild type throughout the life cycle (Fig. 2, C and D; Supplemental Table S1). For example, the rosette diameters of 30-d-old *rpt2a-2* and *rpt2a-3* plants were $30\% \pm 10\%$ larger than in Col-0 (7.8 ± 0.3 , 10.3 ± 0.4 , and 10.4 ± 0.2 cm for Col-0, *rpt2a-2*, and *rpt2a-3*, respectively). Mature *rpt2a* siliques were approximately 30% longer and contained seeds with a 1.4-fold larger area compared with the wild type (Fig. 2D; Supplemental Table S1). The seed number per

silique, however, was reduced in both mutants by approximately 20% (51 ± 4 , 40 ± 3 , and 38 ± 3 for Col-0, *rpt2a-2*, and *rpt2a-3*, respectively; $n \geq 8$, $P \leq 0.005$) due to a reduction in the number of ovules to approximately 80% of the wild-type level (52 ± 2 , 40 ± 7 , and 41 ± 5 for Col-0, *rpt2a-2*, and *rpt2a-3*, respectively; $n \geq 3$, $P \leq 0.005$). Analyses of the morphometric data showed not only that the size of aerial organs in the *rpt2a* mutants was increased but also that organ shapes differed from those of the wild type. In cotyledons, leaves, and petals, for example, the length-to-width ratio in the mutants was larger than in the wild type (Supplemental Table S1). The length-to-width ratios for juvenile leaves (leaves 1 and 2) of 30-d-old plants were 1.1 ± 0.1 , 1.7 ± 0.3 , and 1.4 ± 0.2 for Col-0, *rpt2a-2*, and *rpt2a-3*, respectively. Taken together, these results indicate that loss of function of the *RPT2a* gene affected the mechanisms that determine the final organ size. In addition, the data suggest that the *rpt2a* mutations affect differently those mechanisms that govern proximodistal (i.e. length-related) and medio-lateral (i.e. width-related) control of leaf expansion. Since the establishment of organ polarity was affected in a similar manner in cotyledons, leaves, and flower organs, we also concluded that the affected mechanisms are general and not organ specific.

It should be noted that the increase in *rpt2a* rosette size is not observed when plants are grown on half-strength Murashige and Skoog medium (MS/2 medium; Kurepa et al., 2008). Although we currently do not know what causes this growth difference, one explanation relates to the difference in salt concentrations between the MS/2 medium and soil and the hypersensitivity of 26SP mutants to stresses that cause protein misfolding, such as salt stress.

Kinematic Analyses of Cotyledon Growth in the *rpt2a* Mutants

The final size of an organ depends on the number and size of its cells (Mizukami, 2001). Cell number and cell volume depend on the rate and the duration of cell proliferation and elongation phases but also on compensation, a still unknown mechanism that coordinates cell proliferation and elongation during organ morphogenesis (Tsukaya, 2008). To determine which of the organ size determinants are affected in the *rpt2a* mutants, we first measured the length of the growth period of cotyledons (Fig. 3). The postgermination growth of cotyledons is mostly based on cell expansion. Total cell number per cotyledon has been shown to increase by approximately 30% after 3 d of growth, after which no further cell division has been detected (Tsukaya et al., 1994; Stoyanova-Bakalova et al., 2004). Thus, analyses of cotyledon growth rates should allow us to distinguish between proliferation and elongation and to determine whether the elongation rate or the duration of the elongation phase contributes to the increase in final cotyledon size in the mutants. The time course analyses suggested that the duration of

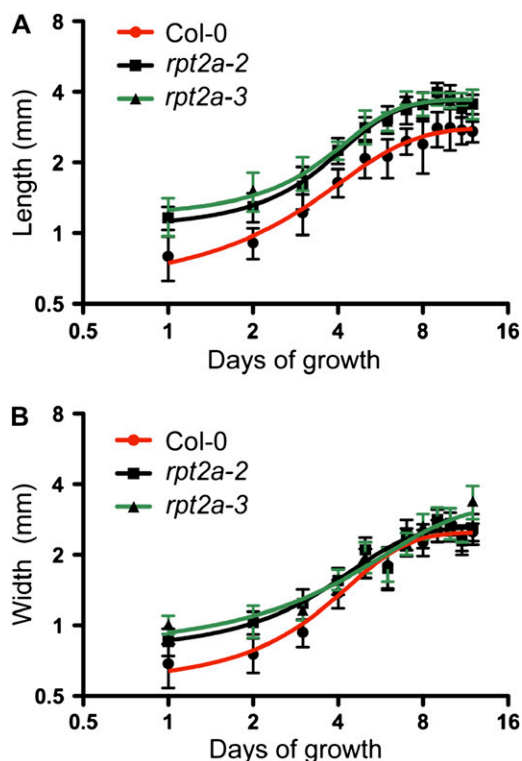


Figure 3. Cotyledon growth in the wild type and *rpt2a* mutants. Plants were grown on MS/2 plates for 2 weeks under a long-day photoperiod. Length (A) and width (B) of 20 or more cotyledons were measured daily. Data are plotted on a \log_2 - \log_2 scale. All data are presented as means \pm SD, and the curves represent nonlinear curve fitting of data using a sigmoidal model with variable slope.

longitudinal growth of wild-type and mutant cotyledons was nearly identical; in all lines, the growth curves reached a plateau after 8 d (Fig. 3A). Thus, the increased final cotyledon length in the mutants was not due to extended postgermination expansion growth and reflected the size differences already established during embryogenesis. The lateral growth period for the wild type and the *rpt2a-2* mutant was also nearly identical, ending around day 8, whereas the *rpt2a-3* mutant cotyledons displayed a modest expansion beyond this time point (Fig. 3B). The longitudinal and especially lateral growth rates differed between the mutants and the wild type. The HillSlope coefficients that describe the steepness of the growth curves were 0.24 ± 0.05 , 0.36 ± 0.07 , and 0.36 ± 0.05 for longitudinal growth and 0.31 ± 0.05 , 0.18 ± 0.07 , and 0.15 ± 0.06 for lateral growth curves of Col-0, *rpt2a-2*, and *rpt2a-3*, respectively. The faster proximodistal expansion and reduced mediolateral expansion in *rpt2a* mutants explain the increased length-to-width ratio of their cotyledons (Supplemental Table S1).

To test if the increased cotyledon size in the mutants is a result of increased cell size, cell number, or both, we analyzed the cell sizes and numbers in cotyledons of mature embryos and 3- and 10-d-old light-grown

seedlings (Fig. 4). In mature *rpt2a* embryos, the cells of the adaxial palisade layer from the central part of the cotyledons were larger than in the wild type (Fig. 4, A and B). The overall cell numbers per cotyledon, however, were not significantly different (Fig. 4C), which would account for the increased cotyledon area. Measurement of cell sizes and cell numbers in cotyledons of 3- and 10-d-old plants showed that while the cells remained larger, their number was reduced in both mutants when compared with the wild type (Fig. 4, D–G). Thus, the *rpt2a* mutations affect the postgerminative cell proliferation in cotyledons on the one hand and cell sizes during all phases of development on the other. The increase in cell size in an organ accompanied by a reduced cell number is a characteristic of compensation mutants, and because the final organ size in *rpt2a* alleles is increased compared with the wild type, the *rpt2a* mutants can be classified as large-leaf compensation mutants, as defined by Horiguchi et al. (2006).

Cell Sizes and Cell Numbers in Petals of *rpt2a* Mutants

It has been shown that the compensation phenomenon occurs in determinate organs such as cotyledons, leaves, and petals but not in indeterminate organs such as roots (Ferjani et al., 2007). To test if other enlarged determinate organs in *rpt2a* mutants also display compensation of the decreased cell number by increased cell volumes, we analyzed the cells of mature petals. The ridged cells of the adaxial surface of mature petal blades of the mutants had an approximately 3-fold larger area (Fig. 5, A and B), and their total number per petal was reduced to $70\% \pm 10\%$ of the wild type (Fig. 5C). Interestingly, the decrease in total cell number was due solely to a decrease in the cell numbers of the mediolateral plane by approximately 30% (data not shown). In addition to the petal cells, and excepting pollen grains, we observed cell size increases in all other organs of the Arabidopsis shoot that were analyzed (i.e. rosette leaves, siliques, and stems), suggesting that this is a general cellular phenotype associated with *rpt2a* mutants (data not shown).

Polypliodization of Cells in Determinate Organs of *rpt2a* Mutants

The final size of plant cells is often positively correlated with their ploidy level (Mizukami, 2001). Another parameter that has been shown to positively correlate with ploidy levels is the number of trichome branches (Hulskamp, 2004). In Col-0 plants, most trichomes on the adaxial side of the first leaf pair have three branches and a small number (approximately 5%) have four (Fig. 5D). In contrast, more than 40% of trichomes in *rpt2a* mutants had four or more branches (Fig. 5D).

Thus, both the cell size and the trichome morphology of *rpt2a* mutants suggested an overall increase in

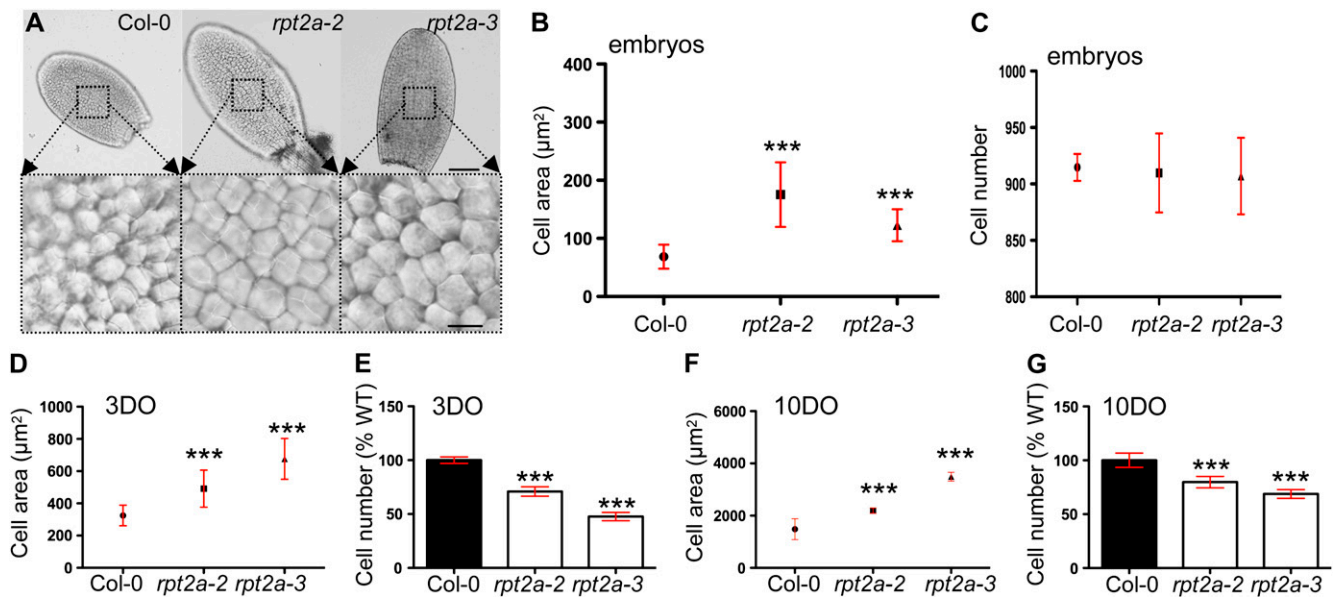


Figure 4. Cell sizes and cell numbers in cotyledons of the wild type and *rpt2a* mutants. A, Cleared cotyledons of mature embryos and close-ups of the central regions showing the sizes of the adaxial subepidermal cells. Bars = 100 μm and 10 μm for top and bottom panels, respectively. B, Average area \pm SD of adaxial subepidermal cells of mature embryos. C, Cell number per cotyledon. The number of palisade cells was counted from micrographs of cleared cotyledons. A minimum of five cotyledons per line was analyzed, and the mean \pm SD is shown. D and E, Cell area (D) and cell number (E) in unexpanded 3-d-old (3DO) cotyledons. The number of adaxial subepidermal cells per cotyledon is presented as mean \pm SD, and the cell number is presented relative to the wild-type (WT) values \pm SD. F and G, Cell area (F) and cell number (G) in fully expanded, 10-d-old (10DO) cotyledons. *** $P < 0.0001$. [See online article for color version of this figure.]

ploidy levels. To test the ploidy levels in cells of an organ at different stages in development, we isolated nuclei from unexpanded and mature cotyledons (Fig. 6, A and B). In immature cotyledons dissected from 3-d-old seedlings, we detected a significant increase in 8C and 16C nuclei in both *rpt2a* mutants (Fig. 6A). It has been shown that the overall proportion of cells with higher ploidy levels (4C, 8C, 16C, and 32C) increases with the age of *Arabidopsis* tissues (Galbraith et al., 1991). Indeed, in fully expanded cotyledons dissected from 10-d-old seedlings, we observed nuclei in five ploidy classes, from 2C to 32C, in both wild-type and mutant lines (Fig. 6B). In mutants, however, the number of cells that contained highly polyploid nuclei was significantly higher than in the wild type (Fig. 6B). The endoreduplication factor (EF), which measures the average number of endocycles per 100 cells (Cookson et al., 2006), was 109.1 ± 1.1 , 135.3 ± 2.4 , and 145.2 ± 0.9 for 3-d-old Col-0, *rpt2a-2*, and *rpt2a-3* cotyledons, respectively, and 200.5 ± 4.5 , 227.5 ± 2.5 , and 223.6 ± 4 for cotyledons of 10-d-old Col-0, *rpt2a-2*, and *rpt2a-3* plants. The differences between the Col-0 EF and the EFs of the *rpt2a* mutants were statistically significant ($P < 0.005$), suggesting that there is a positive correlation between ploidy level, cell size, and organ size in cotyledons.

To further test if the cell size increases in the *rpt2a* mutants are correlated with increased ploidy levels, we measured the DNA content of cells of two other

organs that are enlarged in both mutants. First, we measured the DNA content of petal cells (Fig. 6C). Previous studies have shown that cells at the tip of the petal blade are predominantly diploid (Hase et al., 2005), while DNA content analyses of the entire organ (i.e. the petal blade and claw) showed some polyploidization (Dewitte et al., 2007). We measured the ploidy distribution in whole petals of flowers at stage 15 (Smyth et al., 1990). Surprisingly, the distribution of ploidy classes in the mutants was almost identical to that of the wild type (Fig. 6C). The EFs were 33.3 ± 2.1 , 35.4 ± 1.5 , and 38.9 ± 1.9 for Col-0, *rpt2a-2*, and *rpt2a-3*, respectively. In petals, therefore, there was no significant correlation between cell size and ploidy level. Finally, we also analyzed the relationship between the overall size and ploidy level of cells in hypocotyls of the wild type and mutants. Hypocotyls of 3-d-old *rpt2a* mutant seedlings grown in the dark were longer and thicker compared with the wild type (Supplemental Table S1) and also contained larger cells (data not shown). However, although the distributions of ploidy classes were altered in both mutants, the overall ploidy levels were not increased (Fig. 6D). In fact, the EFs of the mutants were lower than that in the wild type (201.7 ± 3.5 , 179.1 ± 3.8 , and 163.4 ± 6.2 for Col-0, *rpt2a-2*, and *rpt2a-3*, respectively). We concluded that in *rpt2a* mutants, similar to *fugu* compensation mutants (Ferjani et al., 2007), cell and organ enlargement was not correlated with increased endoreduplication.

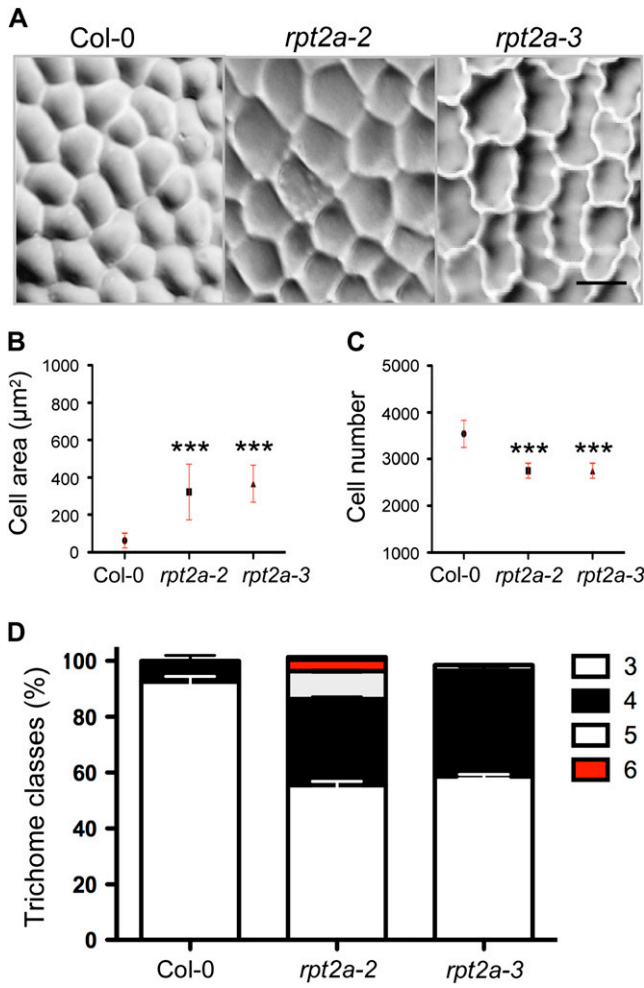


Figure 5. Cell sizes in petals and trichome branch numbers. A, Mature petals of the wild type and *rpt2a* mutants were analyzed using the method of Horiguchi et al. (2006). Ridged epidermal cells from the central region of petals are shown. Bar = 20 μm . B, The average cell area was measured in petals dissected from 10 flowers at stage 15. *** $P < 0.0001$. C, The cell number per petal was counted from at least three petals. The data are presented as means \pm SD. *** $P < 0.0001$. D, Increased trichome branching in *rpt2a* mutants. A minimum of 120 trichomes per line were analyzed in rosette leaves 3 and 4, and the frequency of trichomes with three, four, five, six, and seven branches is presented as the percentage of the total number of trichomes counted. [See online article for color version of this figure.]

Cell Sizes, Cell Numbers, and Ploidy Levels in Other RP Mutants

While the general size increases of *rpt2a* shoot organs sets these mutants apart from other 26SP RP mutants, it remained possible that this phenotype merely reflects a different degree in proteasome malfunction than a specific function of RPT2 within the particle. To test this possibility, we analyzed two other RP mutants that carry more severe defects in proteasome function. The proteasome activity levels and development of the RP mutants *rpn10-1* and *rpn12-1*

have been described previously (Smalle et al., 2002, 2003; Kurepa et al., 2008). The 26SP activity is decreased to approximately 30% of the wild-type level in *rpn10-1* and to approximately 40% in *rpn12a-1* (Kurepa et al., 2008). Thus, if the cellular phenotypes that we observed for *rpt2a* mutants are a result of a general decrease in 26SP function, they should be even more pronounced in the *rpn10-1* and *rpn12a-1* lines, given

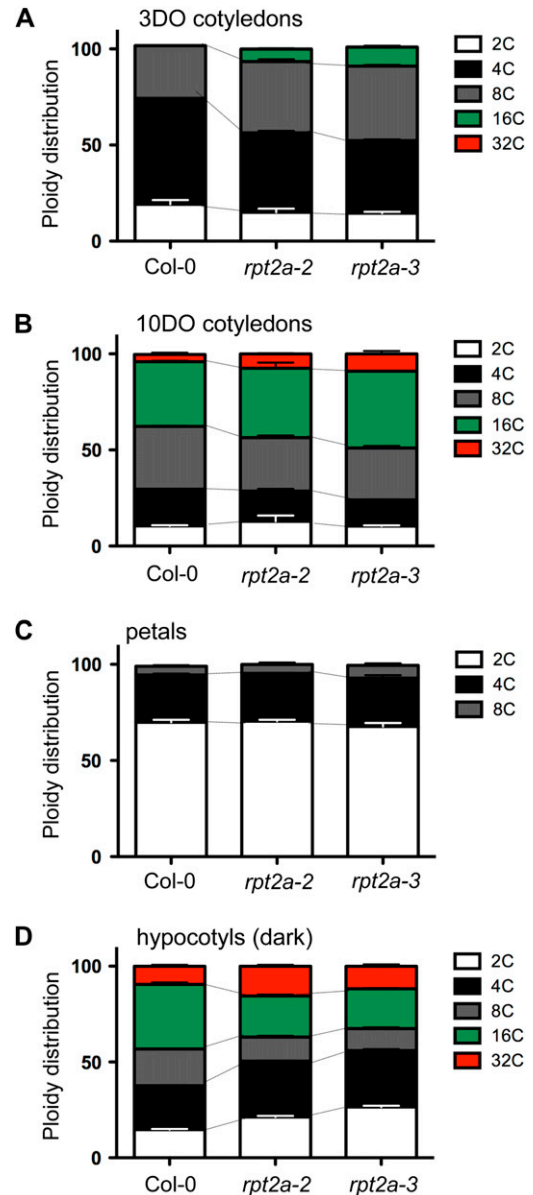


Figure 6. Quantification of the distribution of ploidy levels in *rpt2a* mutants. A and B, Relative ratio of ploidy classes in unexpanded 3-d-old (3DO) and mature 10-d-old (10DO) cotyledons. Twenty cotyledons were pooled for each measurement, and measurements were repeated at least two times. Error bars indicate SD. C, Ploidy distribution in petals was determined by isolating nuclei from petals dissected from at least 10 mature flowers. Mean values \pm SD are shown. D, Ploidy distribution in hypocotyls of 3-d-old etiolated seedlings.

that the *rpt2a-2* mutation only caused a reduction to approximately 60% of the wild-type 26SP activity (Kurepa et al., 2008). The most obvious developmental phenotypes of *rpn10-1* and *rpn12a-1* are shorter roots and smaller rosettes (Smalle et al., 2002, 2003; Kurepa et al., 2008). However, some shoot organs in *rpn10-1* and *rpn12a-1* are larger than in the wild type. In *rpn12a-1*, flowers and cotyledons are larger, while in *rpn10-1*, only flowers are enlarged (Fig. 7, A and E; Smalle et al., 2003). Thus, any level of decrease in 26SP function leads to an inhibition of root development, while the effects on shoot organ size appeared to be dose dependent and organ specific.

Next, we tested whether organ size in both RP mutants is correlated with cell size and ploidy level. We analyzed cotyledons, which are similar to wild-type size in *rpn10-1* and larger in *rpn12a-1* seedlings, and flowers, which are larger than the wild type in both RP mutants (Fig. 7, A and E). In contrast to *rpt2a*

(Fig. 4B), the total number of palisade cells was also reduced in cotyledons of *rpn10-1* and *rpn12a-1* embryos (Fig. 7B) and remained lower than in the wild type throughout cotyledon development (data not shown). Similar to *rpt2a* mutants, cells of *rpn10-1* and *rpn12a-1* were enlarged at all stages of cotyledon development (Fig. 7C; data not shown). Because the *rpn10-1* mutation leads to a stronger defect in proteasome function, a likely explanation for the absence of any size increase in mature cotyledons is that the cell proliferation rate both during embryogenesis and during postgermination development is more affected than in *rpn12a-1*. In both mutants, we also detected an increase in polyploid nuclei (Fig. 7D). In 16-d-old Col-0 cotyledons, 12% \pm 2% of cells underwent four or more endoreduplication cycles, while in the mutants, 46% \pm 5% (*rpn10-1*) and 44% \pm 3% (*rpn12a-1*) of cells had a 32C or 64C content. In flowers of both mutants, epidermal cells in petals were larger than those in the wild type (Fig. 7, F

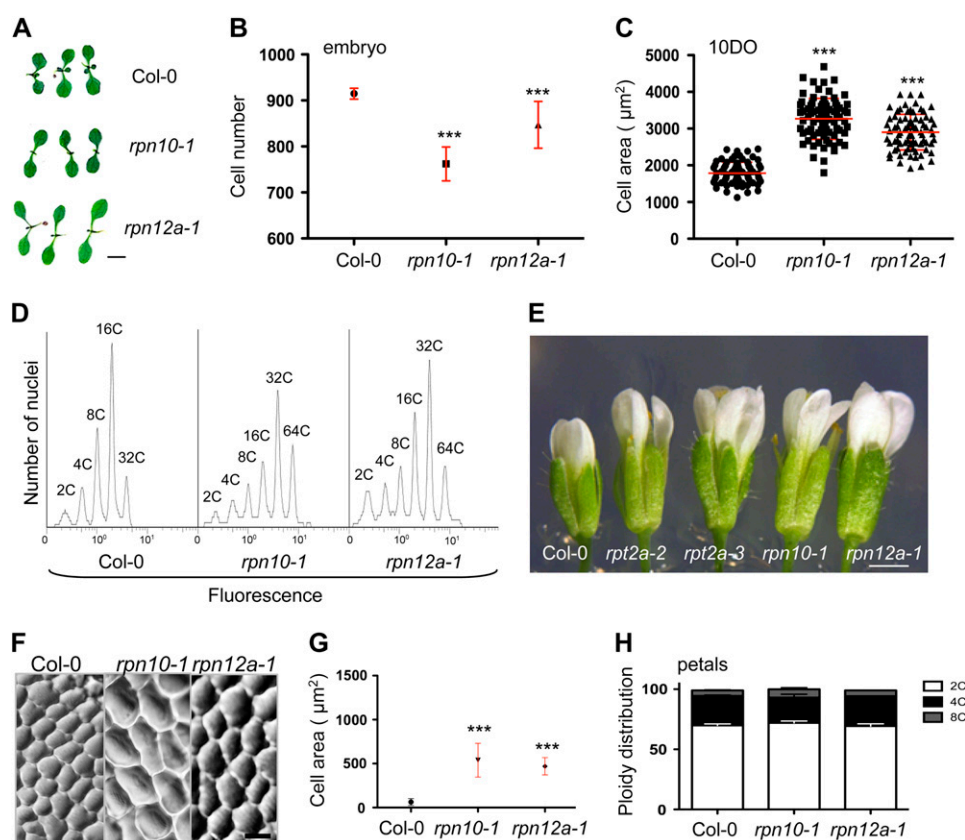


Figure 7. Organ and cell sizes and ploidy levels in *rpn10-1* and *rpn12a-1* mutants. A, Ten-day-old wild-type, *rpn10-1*, and *rpn12a-1* seedlings. Bar = 1 mm. B, The cell number of cotyledons was counted from photographs of lactophenol-cleared mature embryos. Five cotyledons per line were analyzed. C, The size of adaxial parenchymatic cells was determined in 10-d-old (10DO) cotyledons. A minimum of 40 cells were counted from each cotyledon, and 10 cotyledons per line were analyzed. The horizontal line represents the mean, and error bars indicate sd. D, Representative histogram of propidium iodide fluorescence intensity in nuclei isolated from cotyledons of wild-type, *rpn10-1*, and *rpn12a-1* plants grown on MS/2 for 16 d. E, Flowers of RP mutants. Bar = 1 mm. F, Adaxial epidermal cells of wild-type, *rpn10-1*, and *rpn12a-1* petals. Bar = 20 μ m. G, Cell area of adaxial epidermal cells of petals from flowers at floral stage 15. Data are represented as means \pm sd ($n \geq 50$). Asterisks indicate significant differences from the wild type (***) $P < 0.0001$. H, Ploidy distribution in petals was determined as described in the legend to Figure 6C. Mean values \pm sd are shown. [See online article for color version of this figure.]

and G). In addition, the cells of *rpn10-1* were larger than those of *rpn12a-1*. Similar to the *rpt2a* mutants, the increased cell sizes in *rpn10-1* and *rpn12a-1* petals were accompanied by decreases in cell numbers ($51\% \pm 6\%$ and $63\% \pm 9\%$ of the wild type for *rpn10-1* and *rpn12a-1*, respectively). Flow cytometric analyses of the DNA content, however, showed that the ploidy distribution in wild-type and mutant petals also did not differ significantly (Fig. 7H). We conclude that the *rpn10-1* and *rpn12a-1* mutants, similar to *rpt2a* mutants, display a combined decrease in cell proliferation and increase in cell size that is not correlated with nuclear DNA content.

DISCUSSION

Compensation Mechanism of Organ Development and the 26SP

The goals of this study were to determine the cellular basis of shoot organ enlargement in *rpt2a* mutants and to analyze whether the underlying mechanisms reflect a specific function of RPT2a or a general defect in proteasome activity. The mechanisms that control shoot organ size are still largely unknown, in spite of their fundamental importance and economic potential. The current view is that final organ size is controlled by internal developmental signals and modulated by environmental cues (Mizukami, 2001; Tsukaya, 2008). To control final organ size, the intrinsic signaling networks need to control the initiation, duration, and termination of cell proliferation and cell expansion. This implies that these signaling networks are complex and include both promoters and inhibitors of cell division and cell expansion, many of which have been identified (Mizukami and Fischer, 2000; Mizukami, 2001; Hu et al., 2003; Jofuku et al., 2005; Ohto et al., 2005; Disch et al., 2006; Inzé and De Veylder, 2006; Szécsi et al., 2006; Song et al., 2007; Busov et al., 2008). In addition to the networks that regulate cell proliferation and cell expansion, final organ size is controlled by compensation, an integrative system that leads to cell enlargement when the cell number in a determinate organ is reduced (Tsukaya, 2008). Mature cotyledons and petals of the *rpt2a-2*, *rpt2a-3*, *rpn10-1*, and *rpn12a-1* mutants contain fewer cells than those in the wild type, while the average cell volumes are increased. Thus, all tested regulatory particle mutants exhibit compensation. Similar to other mutant or transgenic lines for which compensation phenomena have been described (Inzé and De Veylder, 2006; Ferjani et al., 2007; Tsukaya, 2008), the effects of compensation on final organ size varied considerably within the RP mutant series. For example, petals in all lines were larger than those of the wild type, but the rosette leaves were larger only in the *rpt2a* mutants and smaller in *rpn10-1* and *rpn12a-1*.

The role of ubiquitin/26SP-dependent degradation in the control of cell division has been amply documented (Callis and Vierstra, 2000; Hansen et al., 2002;

Smalle and Vierstra, 2004; Gutierrez and Ronai, 2006; Inzé and De Veylder, 2006; Pines, 2006; Dreher and Callis, 2007; Stone and Callis, 2007). It has also been shown that the strength of the proteasome defect varies considerably within the RP mutant series used in this study (Kurepa et al., 2008). This suggests that in the weakest RP mutants, the *rpt2a* lines, the cell division controls are affected less than in stronger RP mutants, such as *rpn10-1* and *rpn12a-1*. Indeed, while the cell number in expanding cotyledons of young *rpt2a* seedlings was reduced, no reductions were found in cotyledons of mature *rpt2a* embryos, in contrast to the *rpn10-1* and *rpn12a-1* mutants that already showed a lower cell number at this early stage in development (Figs. 4C and 7B). Furthermore, the reduction in cell number in mature petals of all RP mutants was strongest in *rpn12a-1* and *rpn10-1* (Fig. 5C). The compensation phenomenon tends to be observed only in lines in which cell division is decreased below a critical threshold (Tsukaya, 2008). Our results suggest that this compensation threshold has been reached in all RP mutants and that it is predominantly the strength of the cell division defect that determines the final outcome of the compensation effect on organ size. In the weak *rpt2a* mutant lines, combined effects of the decreased cell numbers and compensative cell enlargement led to a general increase in final organ size. In the strong *rpn10-1* mutant, the compensative cell size increases did not lead to enlargement of most shoot organs, probably because of the more severe reductions in cell division activity. This suggests that the growth differences observed between the RP mutants derive from the different strengths of the proteasome defect and are not related to any specific functions that the respective subunits might have within the 26SP particle.

This also suggests that during Arabidopsis shoot development, total 26SP activity needs to be maintained above a critical threshold to ensure the coordinated execution of cell proliferation and expansion programs. This critical threshold must be higher than approximately 60% of the wild-type level, because this activity level in the *rpt2a* mutants was sufficient to trigger a compensation mechanism. This further suggests that fluctuations in total proteasome activity may contribute to the regulation of plant growth. Although our current knowledge of the regulation of proteasome activity in plants is insufficient to support this hypothesis, there is evidence to suggest that proteasome abundance is not maintained at a constant level during the plant life cycle (Kurepa and Smalle, 2008). Recent reports show that proteasome abundance and activity vary during plant development and in response to changes in environmental conditions (Smalle et al., 2002; Itoh et al., 2003; Kim et al., 2003; Shibahara et al., 2004; Yang et al., 2004; Lorenzo and Solano, 2005; Kurepa and Smalle, 2008). These developmental changes in 26SP activity could be an integral component of the regulatory network that controls plant stature, form, and size and may involve, in addition to

effects on cell division and expansion, also developmentally activated plant cell death programs (Kim et al., 2003).

Polyploidy and the 26SP

Similar to its role in cell cycle progression, the role of the ubiquitin/26SP system in the switch from a mitotic cycle to an endoreduplication cycle has been amply documented (Kominami and Toda, 1997; Sigrist and Lehner, 1997; Genschik et al., 1998; Kominami et al., 1998; Cebolla et al., 1999; Szlanka et al., 2003; Neuburger et al., 2006). Here, we show that all RP mutants have altered ploidy profiles in some but not all shoot organs. Because the effect of decreased proteasome function on endoreduplication was organ specific (i.e. it led to an increase in ploidy in cotyledons but not in petals and to a change in ploidy class distribution in etiolated hypocotyls), it confirms previous observations that cells of different tissues and organs express distinct factors that control the mitotic/endoreduplication cycle switch (Churchman et al., 2006). In addition, because the observed changes in cellular DNA content were not correlated with the increased cell and organ sizes, we concluded that the general increase in cell expansion in RP mutants was not driven by increased polyploidization.

26SP- Versus 20SP-Dependent Proteolysis

Numerous studies in plants and animals have described the essential role for 26SP-dependent turnover of cell cycle regulators in controlling the various stages of cell division (Callis and Vierstra, 2000; Hansen et al., 2002; Smalle and Vierstra, 2004; Gutierrez and Ronai, 2006; Inzé and De Veylder, 2006; Pines, 2006; Dreher and Callis, 2007; Stone and Callis, 2007). Accordingly, the cell cycle-related changes in RP mutants can be readily linked to their decreased 26SP activity. However, loss of 26SP function in RP mutants also resulted in increased activity of the free 20SP (Kurepa et al., 2008), and the contribution of this proteolytic pathway to the cellular phenotypes of RP mutants is more difficult to assess. Although some target proteins for the free 20SP have been identified in mammals and yeast, it is currently unclear to what extent this proteolytic pathway contributes to the protein turnover in eukaryotic cells (Asher et al., 2006; Asher and Shaul, 2006). Future studies will have to address to what extent the plant 20SP contributes to the stability control of regulatory proteins, including factors involved in the regulation of cell proliferation, cell expansion, and the mitotic/endoreduplication cycle switch.

MATERIALS AND METHODS

Plant Materials, Growth Conditions, and Treatments

The *rpt2a-3* (SALK_130019) and *rpt2b-1* (SALK_043450C) T-DNA insertion mutants of *Arabidopsis thaliana* were identified in the SIGNAL

collection (Alonso et al., 2003). The *rpt2a-2/nlr-2* (SALK_005596) as well as *rpn10-1* and *rpn12a-1* mutants in the Col-0 background were described previously (Ueda et al., 2004; Kurepa et al., 2008). All plants were grown on MS/2 medium (Sigma), pH 5.7, with 1% Suc and 0.8% phytoagar (RPI Corporation). For soil growth, 7-day-old seedlings were transplanted from MS/2 plates to pots containing 50% Promix and 50% vermiculite. All plants were grown in Conviron growth chambers at 22°C under long-day photoperiods and light of 120 $\mu\text{mol m}^{-2} \text{s}^{-1}$, unless indicated otherwise. MG132 treatments were done as described (Kurepa et al., 2008).

RNA and Protein Analyses

RNA was isolated from 7-d-old seedlings grown in liquid cultures using TRIzol reagent (Invitrogen). Total RNA (10 μg) was separated on 1% agarose-formaldehyde gels, transferred to nitrocellulose membranes (Hybond N+; GE Healthcare), and probed with [^{32}P]UTP-labeled riboprobes synthesized from linearized plasmids using the Riboprobe Combination System (Promega). The antisense *RPT2a* probe was synthesized from *Pst*I-linearized plasmid obtained from the Arabidopsis Biological Resource Center (stock no. 145D18). For immunoblot analyses, plants were weighed, frozen in liquid nitrogen, and ground in two volumes of 2 \times Laemmli sample buffer. Proteins were separated by SDS-PAGE, transferred to nitrocellulose membranes (Hybond C-Extra; GE Healthcare), and probed as described previously (Smalle et al., 2002) using anti-AtRPT2a antibodies purchased from Biomol.

Organ and Cell Analyses

For all morphometric and kinematic analyses, plants or plant organs were photographed and the relevant parameter was measured on digital images using ImageJ (Abramoff et al., 2004). For cotyledon growth curves, a minimum of 30 in vitro-grown seedlings were analyzed. To determine organ size, a minimum of 10 organs were analyzed. For microscopic analyses of embryonic cells and cotyledon palisade cells, tissues were cleared with lactophenol (1:1:1 phenol:water:100% glycerol:lactic acid) for 12 h before analyses. For the analyses of cell sizes and numbers in petals, the printing technique of Horiguchi et al. (2006) was used. A minimum of five cotyledons per line were used to determine cell numbers and cell sizes. Trichome branch numbers were determined using an SZX12 microscope (Olympus).

Flow Cytometry

Nuclei were prepared and stained using the CyStain PI Absolute P kit following the manufacturer's protocol (Partec) and analyzed on a PAS flow cytometer (Partec). A minimum of 20 cotyledons, petals, or hypocotyls per line were pooled for each measurement. The data were analyzed using FlowJo 8.7.5 (Tree Star). Data were derived from at least 10,000 events, and the same gating hierarchy was used for all samples. The propidium iodide-stained nuclei were initially selected on the fluorescence versus the side scatter plot. The nuclear aggregates were then excluded on the forward scatter width versus the side scatter plot. The resulting population was used to analyze DNA content (fluorescence versus number of events).

Statistical Analyses

Descriptive statistics, hypothesis testing, and curve fitting were done using Prism 5.0a software (GraphPad Software). All data are presented as means \pm SD of at least two independent experiments. When means of more than two samples were compared, we used one-way nonparametric ANOVA with the null hypothesis that the value measured in Col-0 equals the value measured in the mutant. When the ANOVA *P* value was less than 0.05, we used the Tukey-Kramer posttest to find a significant difference between pairs of means. The significance levels, indicated by one ($P < 0.05$), two ($P < 0.001$), or three ($P < 0.0001$) asterisks in the figures, illustrate the results of the Tukey-Kramer posttest.

Supplemental Data

The following materials are available in the online version of this article.

Supplemental Table S1. Morphometric characterization of *rpt2a* mutants.

ACKNOWLEDGMENTS

We thank Dr. Tim Phillips (Department of Plant and Soil Science, University of Kentucky) for the use of his Partec PA flow cytometer, Angela Schoergendorfer (Department of Statistics, University of Kentucky) for help with statistical analyses, and the Salk Institute and the Arabidopsis Biological Resource Center for providing the seeds of the *rpt2* mutant lines used in this study.

Received January 20, 2009; accepted March 18, 2009; published March 15, 2009.

LITERATURE CITED

- Abramoff MD, Magelhaes PJ, Ram SJ (2004) Image processing with ImageJ. *Biophotonics Int* 11: 36–42
- Alonso JM, Stepanova AN, Leisse TJ, Kim CJ, Chen H, Shinn P, Stevenson DK, Zimmerman J, Barajas P, Cheuk R, et al (2003) Genome-wide insertional mutagenesis of *Arabidopsis thaliana*. *Science* 301: 653–657
- Asher G, Reuven N, Shaul Y (2006) 20S proteasomes and protein degradation “by default.” *Bioessays* 28: 844–849
- Asher G, Shaul Y (2006) Ubiquitin-independent degradation: lessons from the p53 model. *Isr Med Assoc J* 8: 229–232
- Bajorek M, Glickman MH (2004) Keepers at the final gates: regulatory complexes and gating of the proteasome channel. *Cell Mol Life Sci* 61: 1579–1588
- Benaroudj N, Tarcsa E, Cascio P, Goldberg AL (2001) The unfolding of substrates and ubiquitin-independent protein degradation by proteasomes. *Biochimie* 83: 311–318
- Busov VB, Brunner AM, Strauss SH (2008) Genes for control of plant stature and form. *New Phytol* 177: 589–607
- Callis J, Vierstra RD (2000) Protein degradation in signaling. *Curr Opin Plant Biol* 3: 381–386
- Cebolla A, Vinardell JM, Kiss E, Olah B, Roudier F, Kondorosi A, Kondorosi E (1999) The mitotic inhibitor *ccs52* is required for endoreduplication and ploidy-dependent cell enlargement in plants. *EMBO J* 18: 4476–4484
- Churchman ML, Brown ML, Kato N, Kirik V, Hülskamp M, Inzé D, De Veylder L, Walker JD, Zheng Z, Oppenheimer DG, et al (2006) SIAMESE, a plant-specific cell cycle regulator, controls endoreduplication onset in *Arabidopsis thaliana*. *Plant Cell* 18: 3145–3157
- Cookson SJ, Radziejewski A, Granier C (2006) Cell and leaf size plasticity in Arabidopsis: what is the role of endoreduplication? *Plant Cell Environ* 29: 1273–1283
- DeMartino GN, Gillette TG (2007) Proteasomes: machines for all reasons. *Cell* 129: 659–662
- Dewitte W, Scofield S, Alcasabas AA, Maughan SC, Menges M, Braun N, Collins C, Nieuwland J, Prinsen E, Sundaresan V, et al (2007) *Arabidopsis* CYCD3 D-type cyclins link cell proliferation and endocycles and are rate-limiting for cytokinin responses. *Proc Natl Acad Sci USA* 104: 14537–14542
- Disch S, Anastasiou E, Sharma VK, Laux T, Fletcher JC, Lenhard M (2006) The E3 ubiquitin ligase BIG BROTHER controls Arabidopsis organ size in a dosage-dependent manner. *Curr Biol* 16: 272–279
- Dreher K, Callis J (2007) Ubiquitin, hormones and biotic stress in plants. *Ann Bot (Lond)* 99: 787–822
- Elsasser S, Chandler-Militello D, Müller B, Hanna J, Finley D (2004) Rad23 and Rpn10 serve as alternative ubiquitin receptors for the proteasome. *J Biol Chem* 279: 26817–26822
- Elsasser S, Finley D (2005) Delivery of ubiquitinated substrates to protein-unfolding machines. *Nat Cell Biol* 7: 742–749
- Elsasser S, Gali RR, Schwickart M, Larsen CN, Leggett DS, Müller B, Feng MT, Tübing F, Dittmar GA, Finley D (2002) Proteasome subunit Rpn1 binds ubiquitin-like protein domains. *Nat Cell Biol* 4: 725–730
- Ferjani A, Horiguchi G, Yano S, Tsukaya H (2007) Analysis of leaf development in *fugu* mutants of Arabidopsis reveals three compensation modes that modulate cell expansion in determinate organs. *Plant Physiol* 144: 988–999
- Galbraith DW, Harkins KR, Knapp S (1991) Systemic endopolyploidy in *Arabidopsis thaliana*. *Plant Physiol* 96: 985–989
- Genschik P, Criqui MC, Parmentier Y, Derevier A, Fleck J (1998) Cell cycle-dependent proteolysis in plants: identification of the destruction box pathway and metaphase arrest produced by the proteasome inhibitor MG132. *Plant Cell* 10: 2063–2076
- Gutierrez GJ, Ronai Z (2006) Ubiquitin and SUMO systems in the regulation of mitotic checkpoints. *Trends Biochem Sci* 31: 324–332
- Hanna J, Finley D (2007) A proteasome for all occasions. *FEBS Lett* 581: 2854–2861
- Hansen DV, Hsu JY, Kaiser BK, Jackson PK, Eldridge AG (2002) Control of the centriole and centrosome cycles by ubiquitination enzymes. *Oncogene* 21: 6209–6221
- Hase Y, Fujioka S, Yoshida S, Sun G, Umeda M, Tanaka A (2005) Ectopic endoreduplication caused by sterol alteration results in serrated petals in *Arabidopsis*. *J Exp Bot* 56: 1263–1268
- Horiguchi G, Fujikura U, Ferjani A, Ishikawa N, Tsukaya H (2006) Large-scale histological analysis of leaf mutants using two simple leaf observation methods: identification of novel genetic pathways governing the size and shape of leaves. *Plant J* 48: 638–644
- Hu Y, Xie Q, Chua NH (2003) The *Arabidopsis* auxin-inducible gene *ARGOS* controls lateral organ size. *Plant Cell* 15: 1951–1961
- Huang W, Pi L, Liang W, Xu B, Wang H, Cai R, Huang H (2006) The proteolytic function of the *Arabidopsis* 26S proteasome is required for specifying leaf adaxial identity. *Plant Cell* 18: 2479–2492
- Hulskamp M (2004) Plant trichomes: a model for cell differentiation. *Nat Rev Mol Cell Biol* 5: 471–480
- Husnjak K, Elsasser S, Zhang N, Chen X, Randles L, Shi Y, Hofmann K, Walters KJ, Finley D, Dikic I (2008) Proteasome subunit Rpn13 is a novel ubiquitin receptor. *Nature* 453: 481–488
- Inzé D, De Veylder L (2006) Cell cycle regulation in plant development. *Annu Rev Genet* 40: 77–105
- Itoh H, Matsuoka M, Steber CM (2003) A role for the ubiquitin-26S-proteasome pathway in gibberellin signaling. *Trends Plant Sci* 8: 492–497
- Jofuku KD, Omidyar PK, Gee Z, Okamoto JK (2005) Control of seed mass and seed yield by the floral homeotic gene *APETALA2*. *Proc Natl Acad Sci USA* 102: 3117–3122
- Kim M, Ahn JW, Jin UH, Choi D, Paek KH, Pai HS (2003) Activation of the programmed cell death pathway by inhibition of proteasome function in plants. *J Biol Chem* 278: 19406–19415
- Kominami K, Ochotorena I, Toda T (1998) Two F-box/WD-repeat proteins Pop1 and Pop2 form hetero- and homo-complexes together with cullin-1 in the fission yeast SCF (Skp1-Cullin-1-F-box) ubiquitin ligase. *Genes Cells* 3: 721–735
- Kominami K, Toda T (1997) Fission yeast WD-repeat protein Pop1 regulates genome ploidy through ubiquitin-proteasome-mediated degradation of the CDK inhibitor Rum1 and the S-phase initiator Cdc18. *Genes Dev* 11: 1548–1560
- Kurepa J, Smalle J (2008) Structure, function and regulation of plant proteasomes. *Biochimie* 90: 324–335
- Kurepa J, Toh-e A, Smalle J (2008) 26S proteasome regulatory particle mutants have increased oxidative stress tolerance. *Plant J* 53: 102–114
- Lee H, Zeng SX, Lu H (2006) UV induces p21 rapid turnover independently of ubiquitin and Skp2. *J Biol Chem* 281: 26876–26883
- Lorenzo O, Solano R (2005) Molecular players regulating the jasmonate signalling network. *Curr Opin Plant Biol* 8: 532–540
- Mizukami Y (2001) A matter of size: developmental control of organ size in plants. *Curr Opin Plant Biol* 4: 533–539
- Mizukami Y, Fischer RL (2000) Plant organ size control: *AINTEGUMENTA* regulates growth and cell numbers during organogenesis. *Proc Natl Acad Sci USA* 97: 942–947
- Neuburger PJ, Saville KJ, Zeng J, Smyth KA, Belote JM (2006) A genetic suppressor of two dominant temperature-sensitive lethal proteasome mutants of *Drosophila melanogaster* is itself a mutated proteasome subunit gene. *Genetics* 173: 1377–1387
- Ohto MA, Fischer RL, Goldberg RB, Nakamura K, Harada JJ (2005) Control of seed mass by *APETALA2*. *Proc Natl Acad Sci USA* 102: 3123–3128
- Pande AH, Scaglione P, Taylor M, Nemecek KN, Tuthill S, Moe D, Holmes RK, Tatulian SA, Teter K (2007) Conformational instability of the cholera toxin A1 polypeptide. *J Mol Biol* 374: 1114–1128
- Pines J (2006) Mitosis: a matter of getting rid of the right protein at the right time. *Trends Cell Biol* 16: 55–63
- Rubin DM, Glickman MH, Larsen CN, Dhruvakumar S, Finley D (1998) Active site mutants in the six regulatory particle ATPases reveal multiple roles for ATP in the proteasome. *EMBO J* 17: 4909–4919

- Schmid M, Davison TS, Henz SR, Pape UJ, Demar M, Vingron M, Schölkopf B, Weigel D, Lohmann JU (2005) A gene expression map of *Arabidopsis thaliana* development. *Nat Genet* **37**: 501–506
- Schreiner P, Chen X, Husnjak K, Randles L, Zhang N, Elsasser S, Finley D, Dikic I, Walters KJ, Groll M (2008) Ubiquitin docking at the proteasome through a novel pleckstrin-homology domain interaction. *Nature* **453**: 548–552
- Shibahara T, Kawasaki H, Hirano H (2004) Mass spectrometric analysis of expression of ATPase subunits encoded by duplicated genes in the 19S regulatory particle of rice 26S proteasome. *Arch Biochem Biophys* **421**: 34–41
- Sigrist SJ, Lehner CF (1997) Drosophila fizzy-related down-regulates mitotic cyclins and is required for cell proliferation arrest and entry into endocycles. *Cell* **90**: 671–681
- Smalle J, Kurepa J, Yang P, Babiyhuk E, Kushnir S, Durski A, Vierstra RD (2002) Cytokinin growth responses in *Arabidopsis* involve the 26S proteasome subunit RPN12. *Plant Cell* **14**: 17–32
- Smalle J, Kurepa J, Yang P, Emborg TJ, Babiyhuk E, Kushnir S, Vierstra RD (2003) The pleiotropic role of the 26S proteasome subunit RPN10 in *Arabidopsis* growth and development supports a substrate-specific function in abscisic acid signaling. *Plant Cell* **15**: 965–980
- Smalle J, Vierstra RD (2004) The ubiquitin 26S proteasome proteolytic pathway. *Annu Rev Plant Biol* **55**: 555–590
- Smith DM, Chang SC, Park S, Finley D, Cheng Y, Goldberg AL (2007) Docking of the proteasomal ATPases' carboxyl termini in the 20S proteasome's α ring opens the gate for substrate entry. *Mol Cell* **27**: 731–744
- Smyth DR, Bowman JL, Meyerowitz EM (1990) Early flower development in *Arabidopsis*. *Plant Cell* **2**: 755–767
- Song XJ, Huang W, Shi M, Zhu MZ, Lin HX (2007) A QTL for rice grain width and weight encodes a previously unknown RING-type E3 ubiquitin ligase. *Nat Genet* **39**: 623–630
- Sönnichsen B, Koski LB, Walsh A, Marschall P, Neumann B, Brehm M, Alleaume AM, Artelt J, Bettencourt P, Cassin E, et al (2005) Full-genome RNAi profiling of early embryogenesis in *Caenorhabditis elegans*. *Nature* **434**: 462–469
- Stone SL, Callis J (2007) Ubiquitin ligases mediate growth and development by promoting protein death. *Curr Opin Plant Biol* **10**: 624–632
- Stoynova-Bakalova E, Karanov E, Petrov P, Hall MA (2004) Cell division and cell expansion in cotyledons of *Arabidopsis* seedlings. *New Phytol* **162**: 471–479
- Szécsi J, Joly C, Bordji K, Varaud E, Cock JM, Dumas C, Bendahmane M (2006) *BIGPETALp*, a *bHLH* transcription factor is involved in the control of *Arabidopsis* petal size. *EMBO J* **25**: 3912–3920
- Szlanika T, Haracska L, Kiss I, Deák P, Kurucz E, Andó I, Virágh E, Udvardy A (2003) Deletion of proteasomal subunit S5a/Rpn10/p54 causes lethality, multiple mitotic defects and overexpression of proteasomal genes in *Drosophila melanogaster*. *J Cell Sci* **116**: 1023–1033
- Takahashi M, Iwasaki H, Inoue H, Takahashi K (2002) Reverse genetic analysis of the *Caenorhabditis elegans* 26S proteasome subunits by RNA interference. *Biol Chem* **383**: 1263–1266
- Tsukaya H (2008) Controlling size in multicellular organs: focus on the leaf. *PLoS Biol* **6**: e174
- Tsukaya H, Tsuge T, Uchimiya H (1994) The cotyledon: a superior system for studies of leaf development. *Planta* **195**: 309–312
- Ueda M, Matsui K, Ishiguro S, Sano R, Wada T, Paponov I, Palme K, Okada K (2004) The *HALTED ROOT* gene encoding the 26S proteasome subunit RPT2a is essential for the maintenance of *Arabidopsis* meristems. *Development* **131**: 2101–2111
- Vale RD (2000) AAA proteins: lords of the ring. *J Cell Biol* **150**: F13–F19
- Varshavsky A (2005) Regulated protein degradation. *Trends Biochem Sci* **30**: 283–286
- Wójcik C, DeMartino GN (2002) Analysis of *Drosophila* 26S proteasome using RNA interference. *J Biol Chem* **277**: 6188–6197
- Yang P, Fu H, Walker J, Papa CM, Smalle J, Ju YM, Vierstra RD (2004) Purification of the *Arabidopsis* 26 S proteasome: biochemical and molecular analyses revealed the presence of multiple isoforms. *J Biol Chem* **279**: 6401–6413
- Young P, Deveraux Q, Beal RE, Pickart CM, Rechsteiner M (1998) Characterization of two polyubiquitin binding sites in the 26 S protease subunit 5a. *J Biol Chem* **273**: 5461–5467